Configurable Defected Ground Structures for Low Profile Antenna Performance Enhancement

Yujie Zhang [1], Zixiang Han [1], Shanpu Shen [1], Chi Yuk Chiu [1], and Ross Murch [2]

[1]Affiliation not available
[2]The Hong Kong University of Science and Technology

October 30, 2023

Abstract

Versatile configurable defected ground structures

(CDGSs) for enhancing the performance of low profile antennas are introduced. It is shown that CDGS can significantly reduce mutual coupling (MC) between multiple antennas and suppress cross-polarization (XP) and enhance circular polarization (CP) excitation in single port low profile antennas for example. The key idea of CDGS is to construct defected ground structures (DGSs) from a grid of slots, which can be either opened or shorted with hardwires, so that they can be configured and optimized to enhance desired antenna performance characteristics. The

importance and versatility of the CDGS approach is that it

overcomes the issue of having to design bespoke DGS for each individual antenna design. Three design examples are provided to demonstrate the versatility of CDGSs for MC reduction, XP suppression and CP excitation. Experimental results demonstrate that MC can be reduced by up to 43 dB, XP can be suppressed by 15 dB and CP can be excited with 78 MHz (2.2%) 3-dB axial ratio (AR) bandwidth. The compactness and ease of fabrication also make the CDGS well suited to compact low profile internet of things (IoT) and wireless communication applications.

Configurable Defected Ground Structures for Low Profile Antenna Performance Enhancement

Yujie Zhang, *Student Member, IEEE,* Zixiang Han, *Student Member, IEEE,* Shanpu Shen, *Member, IEEE,* Chi-Yuk Chiu, *Senior Member, IEEE,* and Ross Murch, *Fellow, IEEE*

***Abstract*—Versatile configurable defected ground structures (CDGSs) for enhancing the performance of low profile antennas are introduced. It is shown that CDGS can significantly reduce mutual coupling (MC) between multiple antennas and suppress cross-polarization (XP) and enhance circular polarization (CP) excitation in single port low profile antennas for example. The key idea of CDGS is to construct defected ground structures (DGSs) from a grid of slots, which can be either opened or shorted with hardwires, so that they can be configured and optimized to enhance desired antenna performance characteristics. The importance and versatility of the CDGS approach is that it overcomes the issue of having to design bespoke DGS for each individual antenna design. Three design examples are provided to demonstrate the versatility of CDGSs for MC reduction, XP suppression and CP excitation. Experimental results demonstrate that MC can be reduced by up to 43 dB, XP can be suppressed by 15 dB and CP can be excited with 78 MHz (2.2%) 3-dB axial ratio (AR) bandwidth. The compactness and ease of fabrication also make the CDGS well suited to compact low profile internet of things (IoT) and wireless communication applications.**

***Index Terms*—Circular polarization (CP), cross-polarization (XP), defected ground structure (DGS), linear polarization (LP), multiport antenna, mutual coupling (MC).**

I. Introduction

Low profile antennas such as microstrip patch and planar inverted-F antennas (PIFA) are useful for multiple-input multiple-output (MIMO) communication systems and internet of things (IoT) applications due to their compact size, ease of fabrication and compatibility with integrated circuits [1]. Many techniques have been utilized to enhance the performance of low profile antennas such as parasitic elements [2], electromagnetic band-gap (EBG) structures [3], various feeding methods [4] and defected ground structures (DGSs) [5], [6]. Among all these technologies, DGS can improve antenna performance using only slots etched on the ground plane. A key advantage of the DGS approach is that the original radiating element geometry and location are unchanged with the adoption of DGS.

DGS has been widely used in antenna design for many applications such as mutual coupling (MC) reduction, cross-polarization (XP) suppression, circular polarization (CP) excitation, harmonics suppression and antenna size reduction [7]. However, the design process of DGS is not systematic. It usually requires parametric studies to find the optimum DGS shape and location. Another challenge of the DGS design is its lack of versatility. Most of the previous DGS are only effective for one or two specific applications such as rotationally symmetric slots for MC reduction [6], linear and folded slots for cross-polarization suppression [8], H-slot for harmonic suppression [9], fractal-slot for MC reduction or circular polarization excitation [10], [11].

In this paper, we propose a configurable defected ground structure (CDGS) for enhancing antenna performance. The proposed CDGS consists of a grid of slots etched into the ground plane of the low profile antenna. The length of each slot is less than one tenth of a wavelength and the slots can be shorted or opened using hardwire connections to form a wide variety of DGS geometries. By optimizing the hardwire connections between the slots in the CDGS, a variety of antenna performance characteristics can be optimized. To reduce the computational time for optimizing the CDGS, efficient computational methods can also be optimized [12]-[15]. Unlike other optimization approaches, such as those based on pixel antenna designs [16]-[19], where pixels act as parasitic reactive elements above or around radiating elements, CDGS takes a complementary approach in which slots in the ground plane are used to form DGS patterns to enhance antenna performance. Furthermore, the only other approach utilizing the optimization of slots [20] is for frequency reconfiguration and not for DGS. To the best of the authors' knowledge, this is the first time that configurable slots structures are used as DGS to enhance antenna performance. In particular, this paper provides four main contributions including

1) Proposing a versatile configurable defected ground structure that can enhance low profile antenna characteristics.

2) Deriving an analytical expression for the CDGS impedance and providing an efficient and systematic optimization method for CDGS design.

3) Providing design examples of CDGS for three different applications scenarios for MC reduction, XP suppression and CP excitation.

4) Demonstrating CDGS are compact, easy to fabricate, versatile and provide significant performance enhancement.

In essence, the CDGS approach provides a general systematic approach to the optimization of various low profile antenna characteristics. To support our claim, the effectiveness of the approach are shown by three examples including MC

This work was supported by Hong Kong Research Grants Council under Grant GRF 16209019. *(Corresponding author: Shanpu Shen.)*

Y. Zhang, Z. Han, S. Shen and C. Y. Chiu are with the Department of Electronic and Computer Engineering, The Hong Kong University of Science and Technology, Hong Kong (e-mail: yzhangfy@connect.ust.hk; zhanaj@connect.ust.hk; sshenaa@connect.ust.hk; eefrankie@ust.hk).

R. Murch is with the Department of Electronic and Computer Engineering and Institute for Advanced Study (IAS) at the Hong Kong University of Science and Technology, Hong Kong (e-mail: eermurch@ust.hk).

reduction, XP suppression and CP excitation.

The proposed CDGSs are extremely versatile and therefore a review of previous results for MC reduction, XP suppression and CP excitation also needs to be considered. MC reduction has important applications in MIMO wireless communication systems where antenna coupling degrades antenna efficiency, diversity gain, and channel capacity [10], [21]. Previous approaches to reduce MC have exploited orthogonal-feed methods [22], field canceling parasitic scatter branches [14], [16], [23]-[25], EBG [26], decoupling networks [27]-[29] and DGSs [6], [10], [30]. However, most of the previous work focuses on conventional 2-element decoupling such as [10] and [30] and the proposed structures cannot be effectively extended to more ports. Some existing work such as [6] can deal with MC between four elements but requires a complicated DGS geometry and comprehensive parametric studies. An efficient and systematic design method for DGS suitable for three or more elements therefore needs to be considered and for which our proposed CDGS approach addresses.

The proposed CDGS approach can also be utilized for suppressing XP. In previous work DGS has been widely used for suppressing the XP of microstrip patch antennas and around 15 dB XP reduction in the H-plane has been achieved [8], [31]-[33]. The ring, linear, dot, arc, folded, L-shaped cutting slots on the ground plane can act as "perturbing elements" to alter boundary conditions of some modes which are the main cause of XP radiations. These DGSs can have good XP suppression performance but still need multiple bespoke tuning steps. A systematic method to find the optimum DGS size and performance is therefore again needed and for which CDGS can also fulfill.

The proposed CDGS can also support CP low profile antenna design. CP is important in wireless communication systems for minimizing the polarization misalignment between transmitter and receiver, such as RFID and satellite applications. Various techniques have been proposed to achieve CP on a linearly polarized single-fed microstrip patch antenna such as symmetrical truncated corners [34], asymmetric U-slot [35], CSRR slot [36] and asymmetric-slit corners [37]. All these methods can excite orthogonal modes by changing the physical shape of the radiating elements. Another idea to convert an LP patch antenna to a CP patch antenna is by special feeding networks using apertures and slots [38]-[41]. However, the special feeding structures increase the overall antenna complexity. To the best of the authors' knowledge there are only a few previous results, using DGS to realize CP radiations, without changing the shape or the feeding structure of a square microstrip patch antenna [11], [42], [43]. Our proposed CDGS can provide another approach to alleviating these problems.

The proposed CDGS provides a versatile and general systematic approach to the optimization of various low profile antenna characteristics and the remainder of this paper describes the approach in detail. In Section II, the general concept and theory of CDGS is described. In Section III, an approach to optimizing the CDGS is provided. In Section IV, design examples for MC reduction, XP suppression and CP excitation are given with simulations and measurement results.

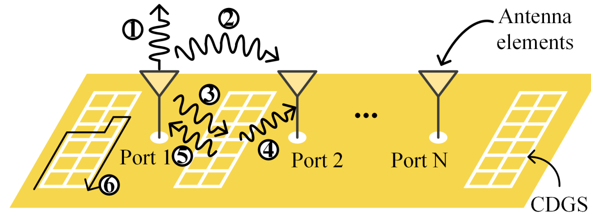

(a)

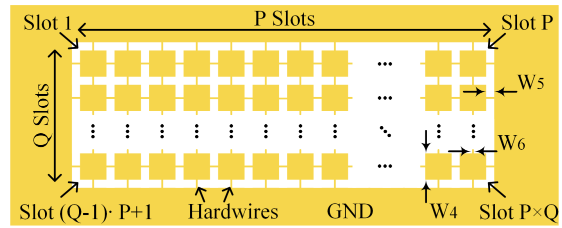

(b)

Fig. 1. Geometry of the CDGS multiport antenna system. (a) Overall geometry where radiation phenomena are shown by the circled numbers and (b) CDGS geometry with $P \times Q$ slots and hardwires.

The MC reduction characteristic is validated through 2-port and 4-port antennas with PIFA arrays. The linear and circular polarizations are realized by a single probe-fed patch antenna using only CDGS. Finally, a conclusion is given in Section V.

In the following sections upper and lower case boldfaced letters are used to represent matrices and vectors respectively. Italic letters are used to represent scalars and elements of vectors and matrices. In addition, for a matrix $\mathbf{X}$, $[\mathbf{X}]^+$ denotes replacing all the negative elements in $\mathbf{X}$ by 0 and $\mathrm{sum}(\mathbf{X})$ denotes the summation of all the entries of the matrix $\mathbf{X}$. The operation $\mathbf{X} \circ \mathbf{Y}$ denotes the Hadamard product (entrywise product) between two matrices with the same dimension. $\mathbf{1}_{M\times N}$ denotes a $M \times N$ matrix with all entries being 1.

II. Geometry and Theory

A. Geometry of CDGS

The geometry for a general CDGS is shown in Fig. 1(a) where N antenna elements with $N+1$ associated CDGS are shown. Each CDGS structure consists of a grid of sub-wavelength slots etched in the ground plane as shown for a general CDGS in Fig. 1(b). Each sub-wavelength slot can be shorted or opened by hardwires so that larger resonant slot structures can be constructed to form a large variety of different possible DGSs. In Fig. 1(b), a grid structure consisting of P by Q slots is shown so that in total there are $P \times Q$ slots and $M = P\times(Q-1)+Q\times(P-1)$ positions for hardwires. If each hardwire can be either opened or shorted in total 2^M possible DGS patterns can be represented by the CDGS. By utilizing optimization, the particular CDGS that enhances a particular antenna characteristic, such as MC, XP or CP, can be found. While Fig. 1 shows the general CDGS, the specific selection of P and Q is described in the design example section that follows.

To illustrate the effect of the CDGS on the antennas, the overall radiation process of the antennas in Fig. 1 can be represented by six phenomena as shown. The first is the conventional radiated space wave as indicated by ①. The second is the coupling of energy to adjacent antennas as indicated by ② and the third is the energy coupled to the CDGS ③. The CDGS can also re-radiate energy from its slots to adjacent antennas ④ as well as back to the original antenna ⑤. Finally the current distribution on the ground plane also affects the antenna characteristics as indicated by the current distribution on the CDGS ⑥.

In compact multiport antennas without DGS, ② is very strong causing strong coupling and low antenna radiation efficiency. When CDGS is integrated, some energy coupled into the slots is re-radiated to adjacent antennas (③ and ④) canceling out the coupling waves (②). Additional slot radiation (⑤) will illuminate the transmitting antenna or space causing minor changes to radiation patterns. When there is only a single antenna, CDGS near the radiating element can change the boundary conditions of the radiating modes by changing the current distribution on the ground (⑥). As a result, some modes can be excited or suppressed enhancing properties such as XP or CP radiating waves. For XP, the boundary conditions of the orthogonal mode can be reduced while for CP, the orthogonal mode can be enhanced to be the same level as the original mode and achieve the necessary 90-degree phase difference.

B. Network Analysis

To perform analysis of the CDGS design, an equivalent circuit model of the CDGS system is depicted in Fig. 2. As illustrated in Fig. 2, the antenna system consists of N feeding ports (numbered 1 to N) and M ports representing the hardwires across the slots in the CDGS (numbered $N+1$ to $N+M$). Thus, the entire network can be represented by a $L \times L$ complex impedance matrix where $L = N + M$. The $L \times L$ complex impedance matrix at frequency f for all the ports is denoted as $\mathbf{Z}(f)$. Each of the N feeding ports is connected to a source with 50 Ω impedance and each of the M CDGS ports is terminated with a hardwire load denoted as z_m^{L} (for $m = 1, \ldots, M$ and the superscript L refers to load). The absence and presence of a hardwire can be modeled by open and short circuits which corresponds to $z_m^{\mathrm{L}} = 0$ or ∞ for all f. Since the load will only have two values, the problem of optimizing the CDGS is a binary optimization problem with M binary variables. Each potential connection state can be represented as $x_m \in \{0,1\}$ (for $m = 1, \ldots, M$) and therefore one specific CDGS configuration, out of all 2^M CDGS states, can be written as $\mathbf{x} = [x_1, x_2, ..., x_M]$.

To simplify the analysis, $\mathbf{Z}(f)$ can be divided into four blocks and written as

$$\mathbf{Z} = \begin{bmatrix} \mathbf{Z}_{\text{Feed}} & \mathbf{Z}_{\text{Feed,CDGS}} \\ \mathbf{Z}_{\text{CDGS,Feed}} & \mathbf{Z}_{\text{CDGS}} \end{bmatrix} \tag{1}$$

where matrix $\mathbf{Z}_{\text{Feed}}$ represents the impedance sub-matrix for the N feeding ports while $\mathbf{Z}_{\text{CDGS}}$ represents the impedance sub-matrix for the M CDGS ports. On the other hand

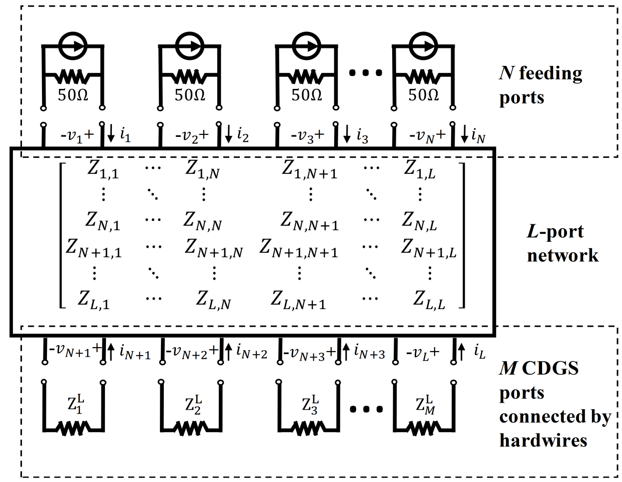

Fig. 2. Circuit model of the CDGS multiport antenna system.

$\mathbf{Z}_{\text{Feed,CDGS}}$ represents the trans-impedance between the voltages of the N feeding ports and the currents of the M CDGS ports. $\mathbf{Z}_{\text{CDGS, Feed}}$ is the transpose of $\mathbf{Z}_{\text{Feed,CDGS}}$. Representing the voltage and current vectors of the feeding and CDGS ports as $\mathbf{v}_{\text{Feed}}$, $\mathbf{v}_{\text{CDGS}}$, $\mathbf{i}_{\text{Feed}}$ and $\mathbf{i}_{\text{CDGS}}$ and using (1), they can be related together by

$$\begin{bmatrix} \mathbf{v}_{\text{Feed}} \\ \mathbf{v}_{\text{CDGS}} \end{bmatrix} = \begin{bmatrix} \mathbf{Z}_{\text{Feed}} & \mathbf{Z}_{\text{Feed,CDGS}} \\ \mathbf{Z}_{\text{CDGS,Feed}} & \mathbf{Z}_{\text{CDGS}} \end{bmatrix} \begin{bmatrix} \mathbf{i}_{\text{Feed}} \\ \mathbf{i}_{\text{CDGS}} \end{bmatrix}. \tag{2}$$

The mth CDGS port is terminated by a hardwire load z_m^{L} as shown in Fig. 2. Therefore,$\mathbf{v}_{\text{CDGS}}$ and $\mathbf{i}_{\text{CDGS}}$ are related by

$$\mathbf{v}_{\text{CDGS}} = -\mathbf{Z}_{\text{Load}} \mathbf{i}_{\text{CDGS}}. \tag{3}$$

where $\mathbf{Z}_{\text{Load}}$ is a diagonal matrix and its (m, m)th entry is z_m^{L}.

Substituting (3) into (2) yields

$$(\mathbf{Z}_{\text{CDGS}} + \mathbf{Z}_{\text{Load}})\, \mathbf{i}_{\text{CDGS}} = -\mathbf{Z}_{\text{CDGS,Feed}} \mathbf{i}_{\text{Feed}}. \tag{4}$$

We use $\mathbf{Z}^A$ to denote the resulting antenna input $N \times N$ impedance matrix when all the CDGS ports have a specific configuration. $\mathbf{Z}^A$ can be written, by substituting (4) into (2) as

$$\mathbf{Z}^A = \mathbf{Z}_{\text{Feed}} - \mathbf{Z}_{\text{Feed,CDGS}} \left(\mathbf{Z}_{\text{CDGS}} + \mathbf{Z}_{\text{Load}}\right)^{-1} \mathbf{Z}_{\text{CDGS,Feed}}. \tag{5}$$

From (5), the final antenna impedance matrix $\mathbf{Z}^A$ consists of the original N-port impedance matrix $\mathbf{Z}_{\text{Feed}}$ and a perturbation term. The perturbation term is affected by the different CDGS patterns on the ground plane (represented by load matrix $\mathbf{Z}_{\text{Load}}$) and demonstrates how the CDGS operates. We can also use $\mathbf{Z}^A$ to determine S-parameters which can then be optimized to fulfill requirements for isolation in multiport antennas.

To optimize XP and CP characteristics we need to extend our results to radiation patterns. Leveraging previous results for efficient calculation of patterns [44], the radiation pattern from a specific feeding port n can be generated by the patterns from each of the individual ports in the structure as

$$E_n^{\theta}(\theta,\varphi)=\sum_{l=1}^{L} i_l E_l^{\theta}(\theta,\varphi) \tag{6}$$

$$E_n^{\varphi}(\theta,\varphi)=\sum_{l=1}^{L} i_l E_l^{\varphi}(\theta,\varphi) \tag{7}$$

where $E_n(\theta,\varphi)$ is the electric field generated by feeding port n; $E_l(\theta,\varphi)$ is the electric field generated by a unit current source with all other ports open; $E^{\theta}(\theta,\varphi)$ and $E^{\varphi}(\theta,\varphi)$ refer to the theta and phi components of the electric field, respectively. The currents $i_1, i_2, ..., i_L$ are port currents when port n is excited. This current distribution can be obtained from (4) with all other feeding ports loaded with 50 Ω and CDGS ports loaded with the designed $\mathbf{Z}_{\text{Load}}$.

The antenna gain and axial ratio (AR) of feeding port n can be calculated from (6) and (7) as

$$G_n(\theta,\varphi)=\frac{4\pi e_{\text{r}} e_{\text{cd}}\left[\left|E_n^{\theta}(\theta,\varphi)\right|^2+\left|E_n^{\varphi}(\theta,\varphi)\right|^2\right]}{\iint\left[\left|E_n^{\theta}(\theta,\varphi)\right|^2+\left|E_n^{\varphi}(\theta,\varphi)\right|^2\right]\sin\theta \mathrm{d}\theta\mathrm{d}\varphi} \tag{8}$$

$$AR_n(\theta,\varphi)=\sqrt{\frac{|E_1|^2+|E_2|^2+|E_1^2+E_2^2|}{|E_1|^2+|E_2|^2-|E_1^2+E_2^2|}} \tag{9}$$

where e_{r} and e_{cd} are antenna reflection (mismatch) efficiency and radiation efficiency, respectively [45]; $E_1(\theta,\varphi)$ and $E_2(\theta,\varphi)$ are tangential components of the selected coordinate system.

III. Optimization

To determine the particular CDGS that enhances the desired antenna performance, hardwire connection optimization is performed using a standard Genetic Algorithm (GA). The objective function, its efficient computation and GA setup is described next.

A. Objective Function

The objective function for enhancing isolation, gain and AR can be expressed as a binary optimization problem as

$$\begin{aligned}\min_{\mathbf{x}}\quad & \sum_{k=1}^{K}\text{sum}\left(\mathbf{W}_{\text{s}}\circ\left[\mathbf{S}(\mathbf{x},f_k)-\mathbf{T}_{\text{s}}\right]^{+}\right)\\ & +\text{sum}\left(\mathbf{W}_{\text{g}}\circ\left[\mathbf{G}(\mathbf{x},f_c,\mathbf{\Omega})-\mathbf{T}_{\text{g}}\right]^{+}\right)\\ & +\text{sum}\left(\mathbf{W}_{\text{ar}}\circ\mathbf{AR}(\mathbf{x},f_c,\mathbf{\Omega})\right)\\ \text{s.t.}\quad & \mathbf{x}\in\{0,1\}^M \end{aligned} \tag{10}$$

where $\mathbf{S}(\mathbf{x},f_k)$ is the $N\times N$ complex scattering matrix of all N feeding ports at frequency f_k with the DGS configurations $\mathbf{x}$; $\mathbf{G}(\mathbf{x},f_c,\mathbf{\Omega})$ is the $N\times R$ gain matrix for the N feeding ports at the center frequency f_c and at R azimuth and elevation angles specified by $\mathbf{\Omega}=[(\theta_1,\varphi_1),(\theta_2,\varphi_2),\ldots,(\theta_R,\varphi_R)]$ in spherical coordinate. The (i,j)th entry of $\mathbf{G}(\mathbf{x},f_c,\mathbf{\Omega})$ is $G_i(\mathbf{x},f_c,\theta_j,\varphi_j)$, which refers to the gain of the ith feeding port at the center frequency f_c and at the jth angle; $\mathbf{AR}(\mathbf{x},f_c,\mathbf{\Omega})$ is also a $N\times R$ real matrix containing the AR of the N feeding ports at the center frequency f_c and R angles specified by $\mathbf{\Omega}$. The (i,j)th entry of $\mathbf{AR}(\mathbf{x},f_c,\mathbf{\Omega})$ is $AR_i(\mathbf{x},f_c,\theta_j,\varphi_j)$, which refers to the AR of the ith feeding port at the center frequency f_c and at the jth angle. $\mathbf{T}_{\text{s}}$ is a $N\times N$ real matrix for the scattering parameter optimization thresholds. $\mathbf{T}_{\text{g}}$ is a $N\times R$ real matrix that contains the gain optimization threshold for each antenna port at angles $\mathbf{\Omega}$. $\mathbf{W}_{\text{s}}$ is a $N\times N$ matrix weight for the scattering term while $\mathbf{W}_{\text{g}}$ and $\mathbf{W}_{\text{ar}}$ are $N\times R$ real matrices for weighing each port's gain and AR terms respectively. It should be noted that when an entry in a weight matrix is negative, it means maximization.

B. Optimization

The optimization process is performed in MATLAB with GA and this has been successfully used in electromagnetic design previously [12], [13], [15]. The impedance matrix $\mathbf{Z}$ and electric fields $E_l(\theta,\varphi)$ are obtained by CST Microwave Studio [46] with only one full-wave simulation. Then, GA optimization is combined with (10) for finding the optimum DGS pattern. Control parameters of GA in this paper are bit string population type, scattered crossover type with 0.8 crossover probability, 0.01 mutation probability, 600 populations and 600 generations as defined in [12].

The computational method is efficient since only one full-wave electromagnetic method is required in the approach. It is over 80$\times$ faster than the optimization process using a full-wave solver at each optimization step. The approach is also related to the Internal Multi-Port Method (IMPM) [12], [17], internal-port method [13], [18], [47] or genetic algorithm/ method of moments (GA/MoM) [15] that have been used for reconfigurable pixel antenna design previously. In the following sections the computational times specified are for a general purpose desktop personal computer.

IV. Design Examples and Results

To verify the versatility and principle of the CDGS for different applications, three design examples are demonstrated in this section. In the first set, examples for 2 and 4-port linearly polarized PIFA arrays are used to validate the CDGS approach for MC reduction. In the second set, a rectangular microstrip patch antenna is chosen as an example for XP suppression. In the third set, CP is excited from a linearly polarized square microstrip patch antenna with only slot etched on the ground plane. All the samples are simulated using CST Microwave Studio and fabricated on RT/Duroid 5880 substrate with dielectric constant and loss tangent of 2.2 and 0.0009, respectively.

A. Mutual Coupling Reduction

1) 2-port Antenna: The geometry of the 2-port PIFA array is shown in Fig. 3 with dimensions in Table. I. The 2-port PIFA array has center-to-center separation of just $0.2\lambda_0$ making it a very compact design and therefore it has very strong coupling making it a challenging example. The details of CDGS can be seen in Fig. 3(b) where its key dimensions are also listed

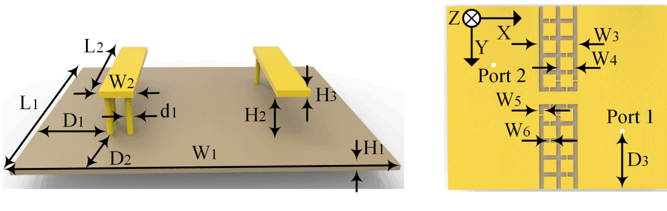

(a) (b)

Fig. 3. Geometry of 2-port PIFA array with proposed CDGS. (a) Perspective view and (b) planar view from underneath showing the optimized CDGS.

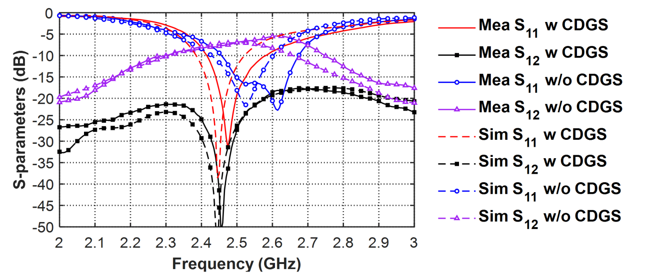

Fig. 4. Simulated and measured S-parameters of 2-port PIFA arrays with and without proposed CDGS.

TABLE I
DIMENSIONS OF 2-PORT ANTENNA ARRAY WITH PROPOSED CDGS

Parameters	W_1	W_2	W_3	W_4	W_5	W_6	L_1	L_2
Length (mm)	52.0	5.0	9.0	3.0	1.0	0.3	43.0	24.2
Parameters	D_1	D_2	D_3	H_1	H_2	H_3	d_1	
Length (mm)	11.5	10.4	13.9	0.8	6.2	0.5	1.0	

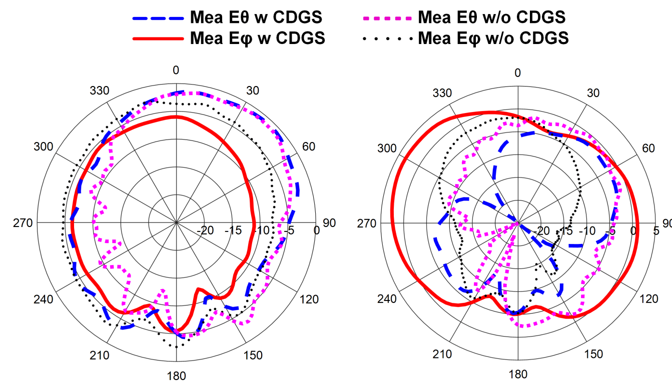

(a) (b)

Fig. 5. Measured Port 1 radiation patterns of 2-port PIFA arrays with and without proposed CDGS in terms of realized gain at 2.45 GHz. (a) E-plane of 2-port PIFA array. (b) H-plane of 2-port PIFA array.

in Table. I. The same CDGS dimensions are used in all the examples in this paper. Since we are dealing with two antennas in this example we also add a connection between the ground planes of both antennas (providing a single common ground plane) and that is why the middle slots of the CDGS are removed and replaced by a solid conductor.

The objective function takes into account S-parameter terms only so that the weight matrix can be written as

$$\mathbf{W}_\mathrm{s} = \begin{bmatrix} 1 & 1 \\ 0 & 0 \end{bmatrix}. \tag{11}$$

Only S_{11} and S_{12} are considered due to symmetry. The other weight matrices are set to zero matrix. The 2-port PIFA array is selected to cover the 2.4 GHz band. Thus, frequency parameters are set with $f_k \in \{2.4, 2.41, 2.42, ..., 2.48\}$. The threshold matrix is then set to be

$$\mathbf{T}_\mathrm{s} = \begin{bmatrix} -10 & -30 \\ -30 & -10 \end{bmatrix}, \tag{12}$$

so that S_{11} and S_{12} should be lower than -10 dB and -30 dB in the entire frequency band of interest, respectively.

As shown in Fig. 3, the 2-port PIFA array has 2 feeding ports so that $N = 2$ and a grid of slots where $M = 50$. We also utilize symmetry in the computation reducing the unknowns in $\mathbf{x}$ to 25 only. The total optimization time and generations needed for optimizing the 2-port PIFA array are 50.6s and 64 respectively. In general, each simulation takes only 0.0013s which is much faster than that of the traditional DGS design method using full-wave simulation based on parametric studies.

Fig. 4 compares simulated and measured S-parameters of the proposed 2-port PIFA array with and without CDGS. Since the 2-port PIFA array is designed with a 6.2 mm air gap with $0.2\lambda_0$ separation, coupling is very strong and the measured S_{12} is -5 dB. The simulated antenna with optimized CDGS has S_{11} lower than -10 dB from 2.38 to 2.52 GHz and S_{12} lower than -30 dB from 2.40 to 2.48 GHz which satisfies the design goal. The measured antenna with CDGS has -10 dB bandwidth from 2.41 to 2.58 GHz with S_{12} lower than -30 dB from 2.43 to 2.49 GHz. The deviation between simulation and measurement can be reduced by using more rigid plates to fabricate the antenna. The comparison between S_{12} with and without CDGS at 2.45 GHz shows that the minimum measured MC is reduced from -7 dB to less than -50 dB giving more than 43 dB reduction in MC. The significant MC reduction demonstrates the decoupling capability of CDGS for strong coupled antennas.

Fig. 5(a) and (b) compare E-plane and H-plane radiation patterns of PIFAs excited at Port 1 with and without CDGS, respectively. Since the two PIFAs are strongly coupled, the radiation pattern is dominated by the coupled fields. Thus, the maximum gain has been increased due to the increase in antenna efficiency using CDGS.

The current distributions on the 2-port PIFA arrays with and without CDGS are given in Fig. 6. For 2-port PIFA array without CDGS, the MC is -7 dB at 2.45 GHz. Thus, the induced current on adjacent PIFA is relatively strong when the other port is excited as shown in Fig. 6(a). It is seen in Fig. 6(b) that the induced current intensity on the passive antenna is significantly reduced when the proposed CDGS is applied. Therefore, the proposed CDGS helps cancel the current between adjacent antenna elements, reducing MC.

2) 4-port Antenna: Most previous decoupling methods focus on 2 elements as they are difficult to extend to more ports [10], [14], [24], [30]. To show the decoupling performance of CDGS for more ports, the PIFA array has been modified from

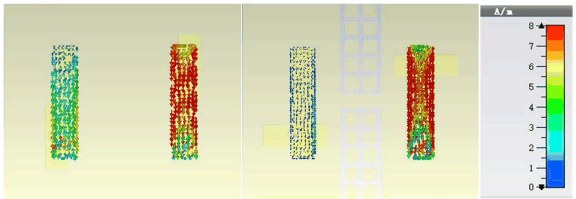

(a) (b)

Fig. 6. Current distributions of 2-port PIFA arrays at 2.45 GHz. (a) Without CDGS. (b) With proposed CDGS.

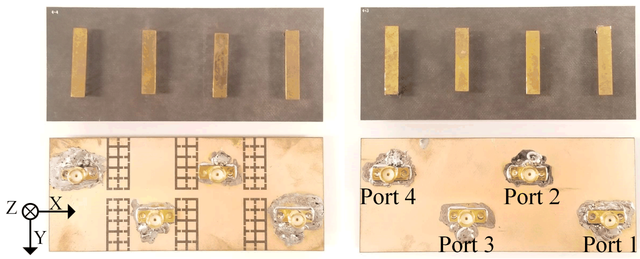

(a) (b)

Fig. 7. Prototypes of 4-port PIFA arrays. (a) With proposed CDGS. (b) without CDGS.

2-port to 4-port with the same center-to-center separation of $0.2\lambda_0$ and with other dimensions also the same. Prototypes are shown in Fig. 7 where it can be observed that the ground planes of each antenna are again connected by replacing the middle slots with a solid ground plane.

A symmetric CDGS can be applied again which reduces the variable digits in $\mathbf{x}$ significantly. The weight matrix can be written as

$$\mathbf{W}_{\mathrm{s}} = \begin{bmatrix} 1 & 1 & 1 & 1 \\ 0 & 1 & 1 & 0 \\ 0 & 0 & 0 & 0 \\ 0 & 0 & 0 & 0 \end{bmatrix} \tag{13}$$

where only S_{11}, S_{12}, S_{13}, S_{14}, S_{22}, S_{23} are taken into consideration due to symmetry. The optimization parameters for the 4-port PIFA array are $L = 154$, $M = 150$, $M_{\mathrm{sym}} = M/2 = 75$ (M reduced by half after using symmetrical structure),

$$\mathbf{T}_{\mathrm{s}} = \begin{bmatrix} -10 & -20 & -20 & -20 \\ -20 & -10 & -20 & -20 \\ -20 & -20 & -10 & -20 \\ -20 & -20 & -20 & -10 \end{bmatrix}. \tag{14}$$

K and f_k are the same as the 2-port case. The optimization time and generations needed are 612.0s and 112 respectively. Thus, each simulation takes only 0.009s.

Fig. 8 compares simulated and measured S-parameters of 4-port PIFA arrays with and without CDGS. The measured S_{12} and S_{23} are reduced from -6.6 to -20.0 dB and from -6.7 to -18.3 dB, respectively which is equivalent to more than 10 dB reduction from 2.40 to 2.48 GHz. The measured non-adjacent elements isolation, S_{13} and S_{14} are maintained low. Both of them are lower than -20 dB in the frequency band of interest. Fig. 9 compares the radiation patterns of the 4-port PIFA arrays with and without CDGS. Same conclusion can be drawn as for 2-port case.

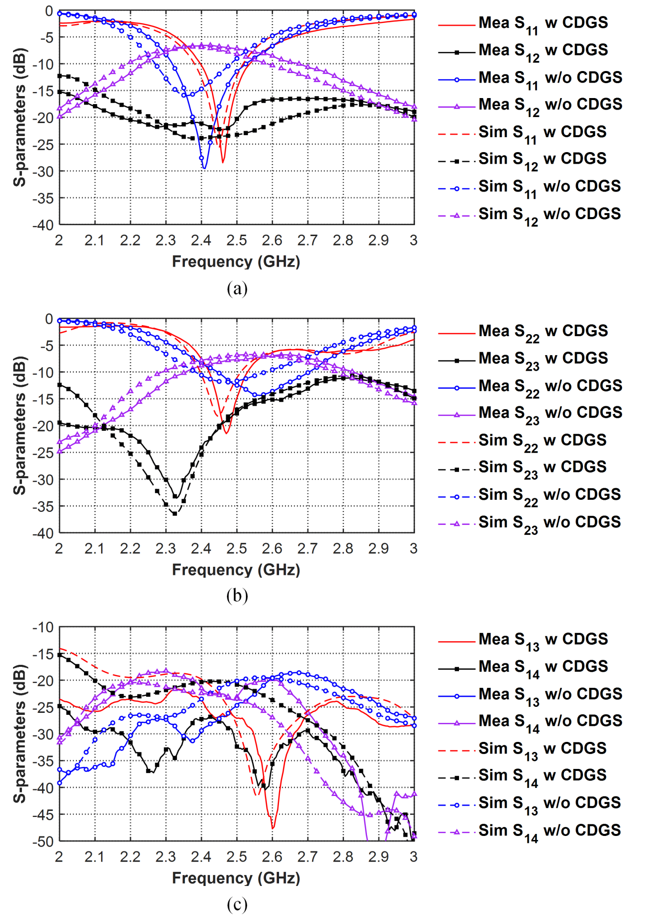

Fig. 8. Simulated and measured S-parameters of the proposed 4-port PIFA arrays with and without proposed CDGS. (a) S_{11} and S_{12}. (b) S_{22} and S_{23}. (c) S_{13} and S_{14}.

Fig. 10 compares total efficiencies of the 2-port and 4-port PIFA arrays with and without CDGS. The significant improvement in antenna efficiencies and S-parameters demonstrate the decoupling capabilities of the CDGS for both 2-port and 4-port designs.

Table. II compares our proposed CDGS decoupling method with other research work for PIFAs and for which there is only one previous example to our knowledge. To be thorough we have therefore also included results for 2-port patch antennas, for which MC was already weak (isolation was already better than -10 dB), which was a focus of much previous work. For proper comparison, we have therefore also included our CDGS approach for a 2-port patch antenna configuration. It can be found that the use of CDGS has advantages in providing high isolation across the frequency band of interest and maintaining good antenna efficiency. Some of the previous decoupling methods only function for a limited bandwidth and are not easy to adjust the operation frequency. Most importantly, CDGS has opened up an approach to multiport antenna MC suppression for antennas with more than 2 ports.

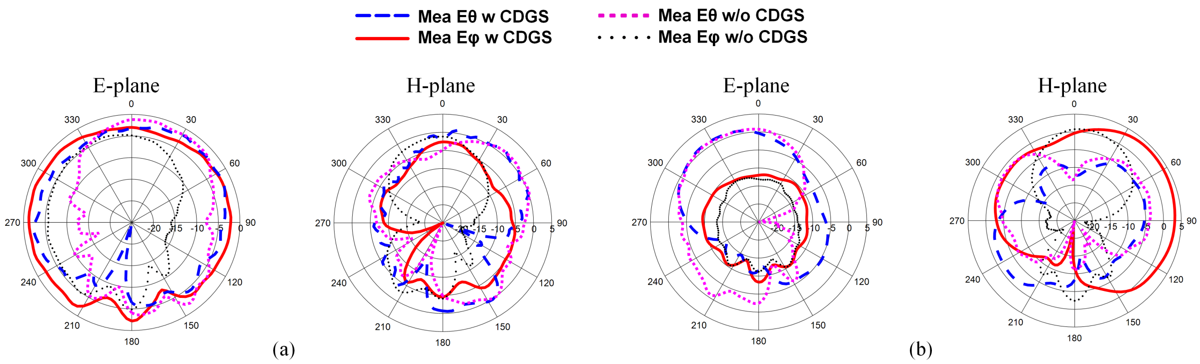

Fig. 9. Measured radiation patterns of 4-port PIFA arrays with and without proposed CDGS in terms of realized gain at 2.45 GHz. (a) Port 1 patterns. (b) Port 2 patterns.

TABLE II
COMPARISON OF MC REDUCTION METHOD AND THEIR PERFORMANCES

Ref.	No. of Ports	Antenna Type	Method	Center Frequency (GHz)	Center-to-center Separation (λ_0)	Max. MC Reduction (dB)	Max. S_{ij} in Frequency Band of Interest (dB)	Antenna Efficiency (%)
[10]	2	Patch	FDGS	2.30	0.38	35 (-15 to -50)	-26 (2.28-2.32 GHz)	N/A
[16]	2	Patch	Parasitic	5.85	0.39	22 (-13 to -35)	-22 (5.70-6.00 GHz)	60
[26]	2	Patch	EBG	5.86	0.88	8 (-17 to -25)	-23 (5.83-5.89 GHz)	N/A
[30]	2	Patch PIFA	SDGS	0.90 2.36	0.27 0.12	11 (-17 to -28) 12 (-6 to -18)	-25 (0.96-0.98 GHz) -18 (2.31-2.40 GHz)	N/A 88
[48]	2	Patch	Parasitic	2.44	0.60	16 (-24 to -40)	-30 (2.40-2.50 GHz)	N/A
[49]	2	Patch	FSRR (DGS)	5.22	0.27	41 (-15 to -56)	-56 (5.20-5.23 GHz)	73
This work	2	Patch PIFA	CDGS	3.70 2.45	0.50 0.21	34 (-16 to -50) 43 (-7 to -50)	-30 (3.62-3.78 GHz) -25 (2.40-2.50 GHz)	95 90
	4	PIFA	CDGS	2.45	0.21	15 (-7 to -22)	-18 (2.40-2.50 GHz)	85

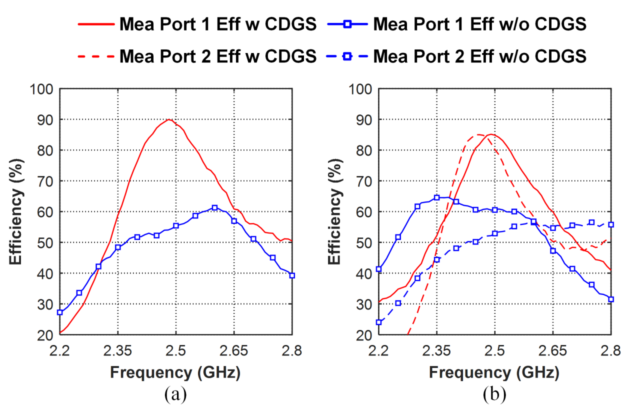

Fig. 10. Measured different multiport antenna efficiencies with and without proposed CDGS. (a) 2-port PIFA array. (b) 4-port PIFA array.

B. Cross-Polarization Suppression

Microstrip patch antennas resonating with $\text{TM}_{\text{m,n}}$ mode are primarily linearly polarized. However, some orthogonal modes exist and create cross-polarization (XP) [50], [51]. It is concluded in [8] and [52] that XP becomes significant for probe-fed microstrip antenna especially when the thickness of the substrate is large. The microstrip patch antenna is inherently narrow band but increasing its thickness can enlarge the bandwidth accordingly. Therefore, reducing XP is important, especially when frequency goes up and substrate thickness remains unchanged. For a rectangular patch antenna, the dominant mode is $\text{TM}_{0,1}$ and the main contribution of XP comes from $\text{TM}_{2,0}$ mode [8]. The radiating orthogonal $\text{TM}_{2,0}$ mode mainly causes the XP in the H-plane and the overall electric fields are not symmetric [33]. To suppress the XP, different types of DGSs are proposed along the radiating sides of the $\text{TM}_{2,0}$ mode altering the boundary condition [8], [33], [53]. However, the process of finding appropriate positions and shapes of these DGSs is time consuming and not efficient.

Utilizing CDGS provides a systematic and efficient way to reduce XP. The geometry of the antenna with CDGS is shown in Fig. 11. Since the electric fields causing XP are symmetric along the y-axis, we also use y-symmetric CDGS with identical slot configurations for the two slots. As a result, the unknowns are again reduced by half.

The mother structure of the proposed antenna consists of one rectangular patch radiator, one feeding port ($N = 1$) and $M = 62$ potential connections. Therefore, the design criteria can be written as a 31 (62/2)-element binary optimization problem with a single objective function (10). The gain matrix can be represented as $\mathbf{G}(\mathbf{x}, f_c, \mathbf{\Omega}) = \left[\mathbf{G}^{\text{XP}}(\mathbf{x}, f_c, \mathbf{\Omega}), G^{\text{Co-P}}(\mathbf{x}, f_c, (0,0))\right]$ where the superscripts XP and Co-P refer to cross-polarization and co-polarization components. The $G^{\text{Co-P}}(\mathbf{x}, f_c, (0,0))$ term is indispensable here, otherwise the XP level can also be reduced just by reducing the total antenna gain. The weights are $\mathbf{W}_{\text{s}} = 1$, $\mathbf{W}_{\text{ar}} = 0$

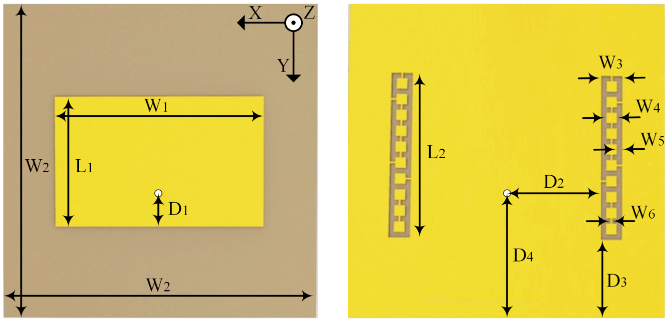

(a) (b)

Fig. 11. Geometry of rectangular patch antenna with proposed CDGS. Dimensions (in mm): W_1 = 39.7, W_2 = 60.0, W_3 = 4.0, W_4 = 2.0, W_5 = 1.0, W_6 = 0.3, L_1 = 24.8, L_2 = 31.0, D_1 = 6.4, D_2 = 17.8, D_3 = 15.0, D_4 = 24.0 and H_{sub} = 3.2 (H_{sub} denotes the thickness of substrate).

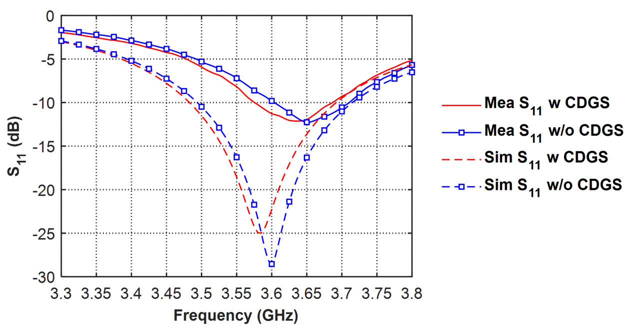

Fig. 12. Simulated and measured S_{11} of LP patch antennas with and without proposed CDGS.

and $\mathbf{W}_g = [\mathbf{1}_{1\times R}, -5]$. The thresholds are $\mathbf{T}_s = -10$ and $\mathbf{T}_g = [-25 \times \mathbf{1}_{1\times R}, 0]$. The frequency index f_c is set to 3.57 GHz and f_k is chosen from 3.5 to 3.7 GHz with steps of 0.01 GHz.

We focus on XP levels in broadside direction in the E-plane and H-plane, so the angular span can be reduced into $\mathbf{\Omega} = \{(\theta_r, \varphi)\,|-70^\circ \le \theta_r \le 70^\circ, \varphi = 0^\circ/90^\circ\}$. The angular step for θ_r is set as 5°, thus $R = 58$ different angular values on E-plane and H-plane are taken. In the constraints, XP levels ($\mathbf{G}^{\mathrm{XP}}$) lower than -25 dB within 140° angular span on E-plane and H-plane are set. The entire optimization process takes 446.4s and converges within 65 generations and is much more efficient than full-wave simulation based on parametric studies. The optimized CDGS geometry is shown in Fig. 11.

Fig. 12 compares simulated and measured S_{11} with and without proposed CDGS. From the simulation results, all samples resonate around 3.57 GHz with more than 200 MHz bandwidth which indicates that CDGS does not affect the bandwidth performance of the antenna. The measured resonance has a frequency shift of 50 MHz compared to the simulation. The deviation mainly comes from the difference between the simulated and experimental substrates, the slight discrepancy in feeding hole size and location, and the soldering. Although the measured bandwidths of the antennas are only 115 MHz, they can be broadened by further enhancing the impedance matching.

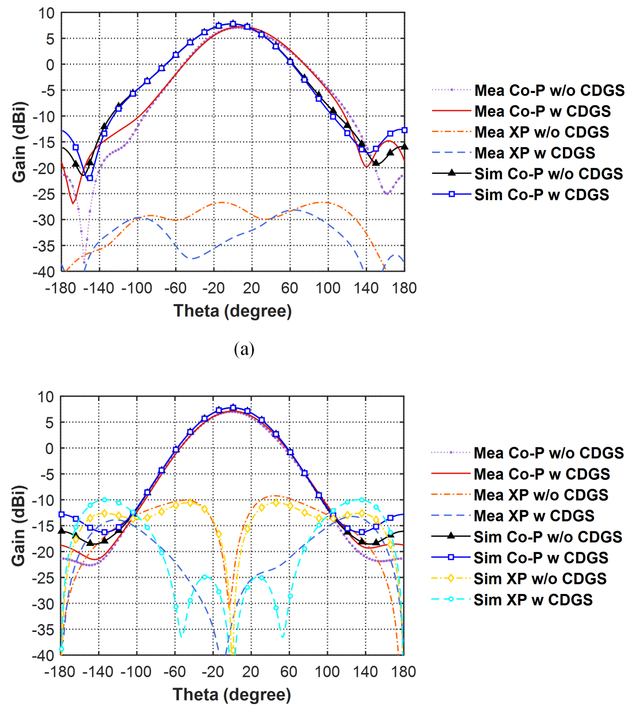

(a)

(b)

Fig. 13. Simulated and measured radiation patterns with and without proposed CDGS in terms of realized gain. (a) E-plane. (b) H-plane.

Fig. 13 compares simulated and measured co-polarization (Co-P) and XP radiation patterns on E-plane and H-plane at their corresponding center frequencies. The simulation results are in good agreement with measurements. The minor deviation for Co-P between simulation and measurement is mainly caused from the loss and dielectric constant difference between ideal model and practical substrate material used. In the objective function, we set the threshold of the XP levels on both E-plane and H-plane as -25 dB from -70° to 70°. From 13(b), it is found that the optimal simulated CDGS can achieve XP level lower than -25 dB from -66° to 66° on H-plane and 15 dB peak XP value reduction within this angular span. Since the simulated XP on E-plane is lower than -100 dB, therefore it cannot be shown in 13(a). The measured XP on H-plane of the antenna with CDGS has 75° angular span lower than -25 dB and also achieve 15 dB peak XP value reduction which shows a significant suppression on XP level. The measured XP on E-plane for the antenna with CDGS is lower than that without CDGS and they are both less than -25 dB in all angles. Figs. 13(a) and (b) show that the Co-P with and without CDGS are the same on both E-plane and H-plane which indicates that the proposed CDGS will not affect the Co-P when the XP level is reduced.

To evaluate the XP suppression performance of the proposed CDGS, the measured H-plane Co-P and XP radiation patterns of antennas with and without proposed CDGS are depicted in Fig. 14 and all gain values have been normalized with the Co-P peak. It can be perceived that the angular span for XP less than -25 dB is originally 22° without DGS and now it can

TABLE III
PERFORMANCE COMPARISON WITH DIFFERENT TYPES OF DGSS FOR SUPPRESSING XP ON PATCH ANTENNAS

Ref.	Antenna Type	Center Frequency (GHz)	DGS Type	Defected Ground Area (λ_0^2)	Angular Span on H-plane with XP < -25 dB Compared to Co-P (°)
[8]	Rectangular patch (W/L=1.6)	10.15	Linear slot	0.100	152
[33]	Rectangular patch (W/L=1.6)	10.10	L slot	0.042	162
[53]	Rectangular patch (W/L=1.5)	9.80	Wide linear slot	0.840	105
[54]	Rectangular patch (W/L=1.6)	10.10	Folded slot	0.054	86
This work	Rectangular patch (W/L=1.6)	3.57	CDGS	0.023	168

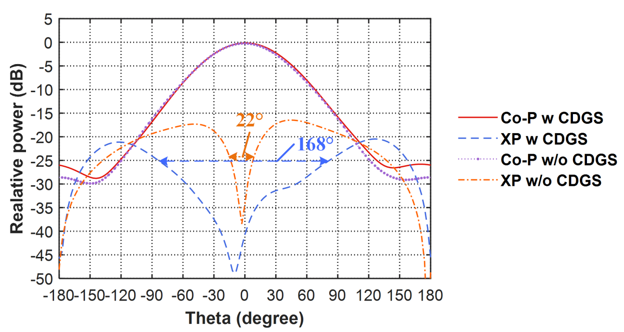

Fig. 14. Measured performance of the CDGS in reducing XP radiation on H-plane.

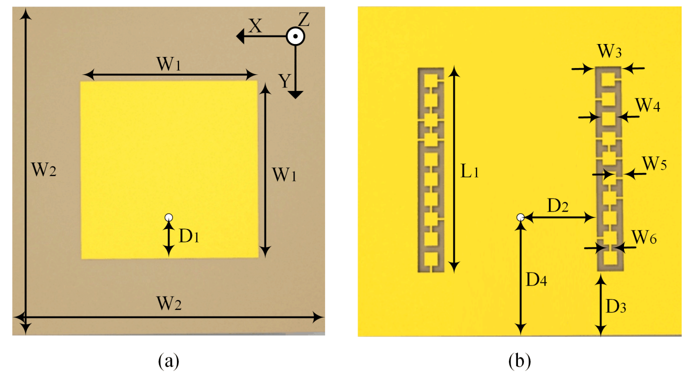

Fig. 15. Geometry of square patch antenna with proposed CDGS. (a) Top view. (b) Bottom view. Dimensions (in mm): W_1 = 27.0, W_2 = 50.0, W_3 = 4.0, W_4 = 2.0, W_5 = 1.0, W_6 = 0.3, L_1 = 31.0, D_1 = 6.5, D_2 = 11.5, D_3 = 9.5, D_4 = 18.0 and H_{sub} = 1.5 (H_{sub} denotes the thickness of substrate).

be significantly enlarged to 168° by applying the proposed CDGS.

A performance comparison between recently proposed DGSs and this work has been provided in Table. III, which shows that the proposed CDGS achieves comparable angular span on H-plane with XP level -25 dB less than the Co-P. Moreover, our work occupies the smallest defected area on the ground plane.

C. Circular Polarization Excitation

Using DGS to excite CP from an LP microstrip patch antenna is not trivial. It needs to enhance the magnitude of an orthogonal mode to the same value as the original mode and attain a 90-degrees phase difference. Traditional U-shaped, Y-shaped and double-bell DGS cannot increase the XP to such a level. A recently proposed fractal-shaped DGS (FDGS) can achieve CP but requires many parametric studies to find the appropriate length of each branch [11]. Inspired by the CDGS suppressing the XP level in the last section, we also study it for increasing XP level and meeting the CP phase requirement for CP excitation. We utilize the same linear CDGS mother structure under the microstrip square patch antenna as the previous XP example, as shown in Fig. 15. However, the left and right slot configurations are not constrained to be symmetrical as in the previous XP example increasing the possible unique hardwire connections (M) from 31 to 62.

The mother structure of the proposed antenna consists of one square patch radiator, one feeding port ($N = 1$) and $M = 62$ potential connections. Thus, the design process can be written as a 62 digits binary optimization problem with a single objective function (10). In this case, the focused beam angle $\mathbf{\Omega} = (\theta = 0°, \varphi = 0°)$ which is the broadside direction of the patch antenna. The weights are $\mathbf{W}_{\text{s}} = 5$, $\mathbf{W}_{\text{g}} = -1$ and $\mathbf{W}_{\text{ar}} = 15$. The thresholds are $\mathbf{T}_{\text{s}} = -10$ and $\mathbf{T}_{\text{g}} = 0$. The frequency index f_c is chosen to be 3.53 GHz and f_k is chosen from 3.52 to 3.54 GHz with steps of 0.01 GHz. The whole optimization takes 145.2s with 70 generations and totally 42000 calculations. Thus, each simulation run takes only 0.0034s. Hence, we can conclude that this DGS design method is much faster than parametric studies on full-wave solvers. The optimal DGS patterns are shown in Fig. 15(b).

Fig. 16 compares the simulated and measured S_{11} of the square patch antenna with and without CDGS. The simulated S_{11} matches well with the measured result. The 40 MHz frequency shift is due to the difference between simulation and practical substrate material and soldering tolerance. We can find that there is only one resonant mode for antenna without CDGS. However, another resonant mode can be excited at the higher frequency band with CDGS. These two resonant modes overlap at 3.53 GHz, which is the center frequency we set for the objective functions. Consequently, the -10 dB bandwidth of the CP antenna is 190 MHz (from 3.48 to 3.67 GHz) which is around twice larger than the original LP antenna with 80 MHz bandwidth (from 3.51 to 3.59 GHz).

The simulated and measured radiation patterns of the proposed CP-CDGS antenna and the reference antenna are depicted in Fig. 17. The measurement results are in good agreement with simulations. It can be found from Fig. 17(a) and (b) that the left-handed circular polarization component dominates in both E-plane and H-plane of the proposed CP-

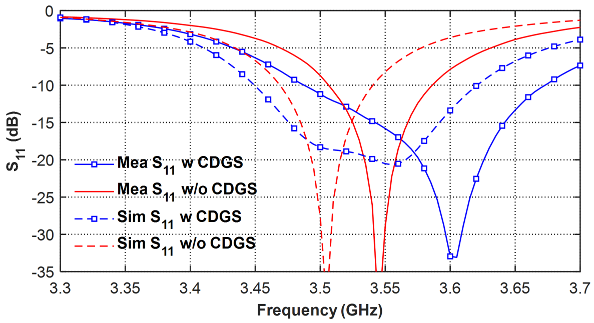

Fig. 16. Simulated and measured S_{11} of square patch antennas with and without proposed CDGS.

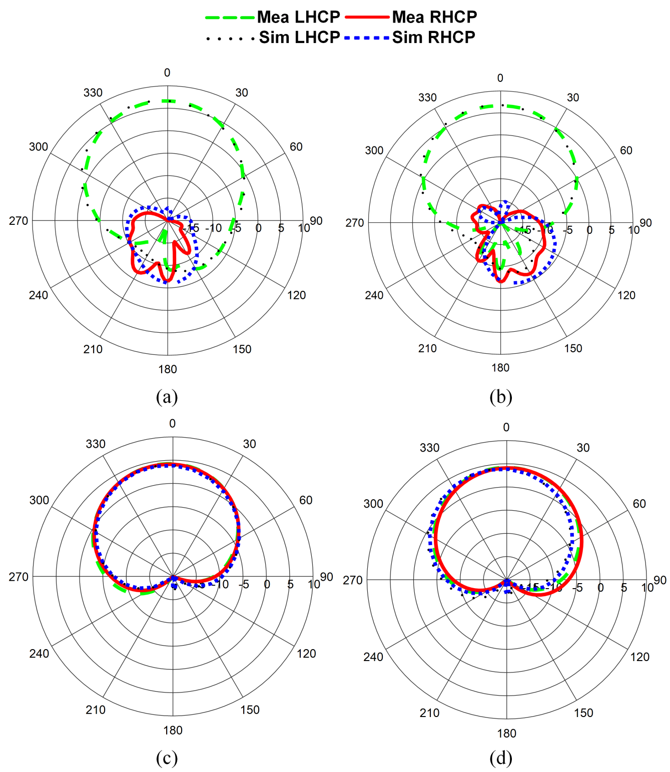

Fig. 17. Measured and simulated radiation patterns of antennas with different ground structures in terms of realized gain at 3.53 GHz. (a) E-plane pattern with CDGS. (b) H-plane pattern with CDGS. (c) E-plane pattern without CDGS. (d) H-plane pattern without CDGS. (Gain unit: dBic)

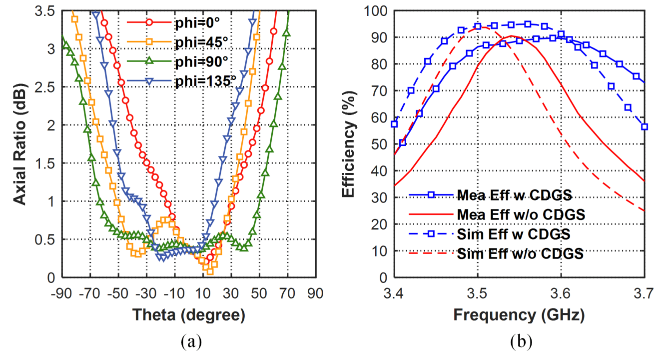

Fig. 18. (a) Measured CP patch antenna's AR versus theta in different phi planes at 3.53 GHz and (b) antenna efficiency versus frequency with and without proposed CDGS.

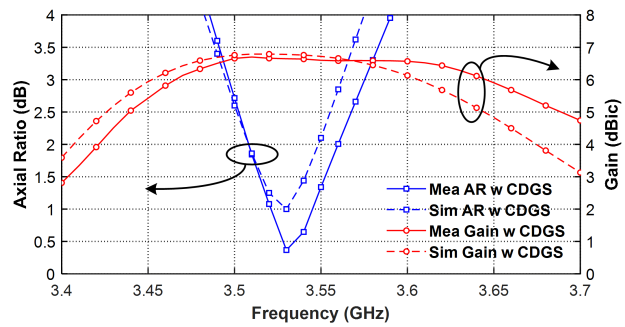

Fig. 19. Simulated and measured CP patch antennas' AR and gain versus frequency in broadside direction.

CDGS antenna. Thus, the proposed CP antenna is left-handed circularly polarized (LHCP). It should be noted that the right and left slot patterns of the CP-CDGS antenna are asymmetric. To change the LHCP antenna to a right-handed circularly polarized (RHCP) antenna, we only need to take a mirror operation of the CDGS configurations between right and left slots. The measured maximum gain of CP antenna is 6.6 dBic. Figs. 17(c) and (d) compare the radiation patterns of the reference LP antenna without CDGS. The RHCP and LHCP components have the same amplitude with maximum gain of 3.9 dBic, which is around 3 dB less than the CP antenna.

Fig. 18(a) shows the proposed CP antenna's AR values versus theta in different phi planes. The 3-dB AR beamwidth is larger than 100 degrees with specific 112, 123, 153, 104 degrees in $\varphi = 0, 45, 90, 135$ planes respectively. The minimum AR value is 0.08 dB at 3.53 GHz $(\theta = 15°, \varphi = 45°)$ which shows the purity of the circular polarization. Fig. 18(b) compares simulated and measured antenna efficiencies with and without CDGS. It can be perceived that the fabricated CDGS sample can achieve highest 90.3% antenna efficiency which is similar to that without CDGS. This result shows that the CDGS does not reduce the antenna efficiency but can enhance the radiation properties. Fig. 19 compares the simulated and measured AR and realized gain of the proposed CP antenna. They are in good agreement. The measured 3-dB AR bandwidth of the proposed LHCP-CDGS antenna is 78 MHz (from 3.497 GHz to 3.575 GHz) or 2.2% of the center frequency 3.53 GHz. The realized CP gain of the proposed CP antenna is stable within its 3-dB AR bandwidth and can achieve maximum 6.6 dBic.

Table. IV compares our proposed CP antenna with previous single-layer single-fed CP patch antenna. It is seen that comparable performance can be achieved in all aspects. The little larger ground size explains the higher gain of our antenna. The 3-dB AR bandwidth and -10 dB impedance bandwidth are related to the height of the antenna. However, the measured 2.2% 3-dB AR bandwidth of our CDGS sample is 5 times larger than recently studied FDGS CP antenna with the same $0.2\lambda_0$ height. Compared with the conventional parametric study method to design DGS for CP excitation, our

TABLE IV
PERFORMANCE COMPARISON OF PROPOSED AND PREVIOUS CP ANTENNA BASED ON SINGLE-LAYER SINGLE-FED PATCH ANTENNA

Ref.	Method	Min. AR Frequency (GHz)	Antenna Size ($\lambda_0 \times \lambda_0 \times \lambda_0$)	Impedance Bandwidth (MHz, %)	3-dB AR Bandwidth (MHz, %)	3-dB AR Beamwidth (°)	Min. AR (dB)	Antenna Realized Gain
[11]	FDGS	1.576	0.24×0.24×0.02	30, 1.90	6, 0.38	90	0.7	2.2 dBic
[35]	U-slot patch	2.320	0.79×0.79×0.09	210, 9.05	90, 3.88	58	0.2	8.0 dBi
[36]	CSRR loaded patch	4.200	0.42×0.42×0.02	200, 4.76	28.5, 0.70	-	1.5	6.2 dBi
[37]	Slit patch	2.405	0.29×0.29×0.01	61, 2.53	12, 0.50	>100	1.6	4.3 dBic
[40]	Cross slot DGS	1.224 1.480	0.24×0.24×0.01	72, 5.88 90, 6.08	12, 0.98 16, 1.08	110 90	0.8	1.4 dBi 3.5 dBi
[42]	L-slot DGS	2.490	0.54×0.65×0.01	110, 4.42	30, 1.20	-	1.90	2.9 dBi
[43]	Loop-slot DGS	2.438	0.65×0.65×0.01	60, 2.46	20, 0.82	-	0.5	6.4 dBi
This work	CDGS	3.530	0.58×0.58×0.02	190, 5.40	78, 2.20	>100	0.08	6.6 dBic

CDGS is more effective. Another advantage of using CDGS in CP antenna design is that we can accurately excite CP at a certain frequency with optimized minimum AR which is hard to realize by other tuning methods.

V. CONCLUSIONS

CDGSs have been proposed and they have been shown to provide significant performance enhancement in low profile antennas including MC reduction, XP suppression and CP excitation. The main advantage of using CDGS is that it provides a systematic and fast design method which is much more efficient than the traditional DGS design approach based on parametric studies. Furthermore, the proposed CDGS can be utilized for multiple applications while a traditional DGS can only function for one or two purposes. Details for three design examples have been provided and the corresponding performance is evaluated and compared with previous work. An efficient method for CDGS optimization is also proposed. In MC reduction an improvement of up to 43 dB has been shown. Furthermore the approach is also effective for MIMO designs with more than 2 antennas. In XP suppression significant increases in angular span with XP less than -25 dB has been demonstrated. For use in CP antenna design, it is demonstrated that 190 MHz (3.48-3.67 GHz) -10 dB bandwidth, 78 MHz (2.2%) 3-dB AR bandwidth and greater than 100° 3-dB AR beamwidth can be achieved. The measured CP gain is stable across the CP band and can achieve 6.6 dBic. The CDGS design method also has potential to be extended to other antenna structures.

ACKNOWLEDGMENT

We gratefully acknowledge the funding support for this research from grant GRF 16209019 provided by the Hong Kong Research Grants Council.

REFERENCES

[1] K. F. Lee, K. M. Luk, and H. W. Lai, *Microstrip patch antennas*. World Scientific, 2017.

[2] S. Wi, Y. Lee, and J. Yook, "Wideband microstrip patch antenna with U-shaped parasitic elements," *IEEE Trans. Antennas Propag.*, vol. 55, no. 4, pp. 1196–1199, Apr. 2007.

[3] J. Lee, S. Kim, and J. Jang, "Reduction of mutual coupling in planar multiple antenna by using 1-D EBG and SRR structures," *IEEE Trans. Antennas Propag.*, vol. 63, no. 9, pp. 4194–4198, Sep. 2015.

[4] P. Li, K. M. Luk, and K. L. Lau, "A dual-feed dual-band L-probe patch antenna," *IEEE Trans. Antennas Propag.*, vol. 53, no. 7, pp. 2321–2323, Jul. 2005.

[5] M. M. Bait-Suwailam, O. F. Siddiqui, and O. M. Ramahi, "Mutual coupling reduction between microstrip patch antennas using slotted-complementary split-ring resonators," *IEEE Antennas Wireless Propag. Lett.*, vol. 9, pp. 876–878, 2010.

[6] C. Y. Chiu, F. Xu, S. Shen, and R. D. Murch, "Mutual coupling reduction of rotationally symmetric multiport antennas," *IEEE Trans. Antennas Propag.*, vol. 66, no. 10, pp. 5013–5021, Oct. 2018.

[7] A. K. Arya, M. Kartikeyan, and A. Patnaik, "Defected ground structure in the perspective of microstrip antennas: a review," *Frequenz*, vol. 64, no. 5-6, pp. 79–84, 2010.

[8] C. Kumar and D. Guha, "Reduction in cross-polarized radiation of microstrip patches using geometry-independent resonant-type defected ground structure (DGS)," *IEEE Trans. Antennas Propag.*, vol. 63, no. 6, pp. 2767–2772, Jun. 2015.

[9] Y. J. Sung, M. Kim, and Y. S. Kim, "Harmonics reduction with defected ground structure for a microstrip patch antenna," *IEEE Antennas Wireless Propag. Lett.*, vol. 2, pp. 111–113, 2003.

[10] K. Wei, J. Li, L. Wang, Z. Xing, and R. Xu, "Mutual coupling reduction by novel fractal defected ground structure bandgap filter," *IEEE Trans. Antennas Propag.*, vol. 64, no. 10, pp. 4328–4335, Oct. 2016.

[11] K. Wei, J. Y. Li, L. Wang, R. Xu, and Z. J. Xing, "A new technique to design circularly polarized microstrip antenna by fractal defected ground structure," *IEEE Trans. Antennas Propag.*, vol. 65, no. 7, pp. 3721–3725, Jul. 2017.

[12] S. Song and R. D. Murch, "An efficient approach for optimizing frequency reconfigurable pixel antennas using genetic algorithms," *IEEE Trans. Antennas Propag.*, vol. 62, no. 2, pp. 609–620, Feb. 2014.

[13] J. Perruisseau-Carrier, F. Bongard, R. Golubovic-Niciforovic, R. Torres-Sanchez, and J. R. Mosig, "Contributions to the modeling and design of reconfigurable reflecting cells embedding discrete control elements," *IEEE Trans. Microw. Theory Techn.*, vol. 58, no. 6, pp. 1621–1628, Jun. 2010.

[14] D. Rodrigo, E. Diaz, and L. Jofre, "Reconfigurable pixel-layer isolator for frequency-tunable on-frequency repeaters," *IEEE Antennas Wireless Propag. Lett.*, vol. 13, pp. 475–478, 2014.

[15] J. M. Johnson and Y. Rahmat-Samii, "Genetic algorithms and method of moments (GA/MOM) for the design of integrated antennas," *IEEE Trans. Antennas Propag.*, vol. 47, no. 10, pp. 1606–1614, Oct. 1999.

[16] Y. Cheng, X. Ding, W. Shao, and B. Wang, "Reduction of mutual coupling between patch antennas using a polarization-conversion isolator," *IEEE Antennas Wireless Propag. Lett.*, vol. 16, pp. 1257–1260, 2017.

[17] S. Soltani, P. Lotfi, and R. D. Murch, "Design and optimization of multiport pixel antennas," *IEEE Trans. Antennas Propag.*, vol. 66, no. 4, pp. 2049–2054, Apr. 2018.

[18] D. Rodrigo, B. A. Cetiner, and L. Jofre, "Frequency, radiation pattern and polarization reconfigurable antenna using a parasitic pixel layer," *IEEE Trans. Antennas Propag.*, vol. 62, no. 6, pp. 3422–3427, Jun. 2014.

[19] S. Shen, C. Y. Chiu, and R. D. Murch, "Multiport pixel rectenna for ambient RF energy harvesting," *IEEE Trans. Antennas Propag.*, vol. 66, no. 2, pp. 644–656, Feb. 2018.

[20] C. Y. Chiu, J. Li, S. Song, and R. D. Murch, "Frequency-reconfigurable pixel slot antenna," *IEEE Trans. Antennas Propag.*, vol. 60, no. 10, pp. 4921–4924, Oct. 2012.

[21] R. Janaswamy, "Effect of element mutual coupling on the capacity of fixed length linear arrays," *IEEE Antennas Wireless Propag. Lett.*, vol. 1, pp. 157–160, 2002.

[22] D. G. Kurup, A. Rydberg, and M. Himdi, "Compact microstrip-T coupled patch antenna for dual polarisation and active antenna applications," *Electron. Lett.*, vol. 38, no. 21, pp. 1240–1241, Oct. 2002.

[23] A. C. K. Mak, C. R. Rowell, and R. D. Murch, "Isolation enhancement between two closely packed antennas," *IEEE Trans. Antennas Propag.*, vol. 56, no. 11, pp. 3411–3419, Nov. 2008.

[24] S. Soltani and R. D. Murch, "A compact planar printed MIMO antenna design," *IEEE Trans. Antennas Propag.*, vol. 63, no. 3, pp. 1140–1149, Mar. 2015.

[25] K. Wu, C. Wei, X. Mei, and Z. Zhang, "Array-antenna decoupling surface," *IEEE Trans. Antennas Propag.*, vol. 65, no. 12, pp. 6728–6738, Dec. 2017.

[26] F. Yang and Y. Rahmat-Samii, "Microstrip antennas integrated with electromagnetic band-gap (EBG) structures: a low mutual coupling design for array applications," *IEEE Trans. Antennas Propag.*, vol. 51, no. 10, pp. 2936–2946, Oct. 2003.

[27] L. Zhao, K. Qian, and K. Wu, "A cascaded coupled resonator decoupling network for mitigating interference between two radios in adjacent frequency bands," *IEEE Trans. Microw. Theory Techn.*, vol. 62, no. 11, pp. 2680–2688, Nov. 2014.

[28] L. Zhao and K. Wu, "A decoupling technique for four-element symmetric arrays with reactively loaded dummy elements," *IEEE Trans. Antennas Propag.*, vol. 62, no. 8, pp. 4416–4421, Aug. 2014.

[29] G. Zhai, Z. N. Chen, and X. Qing, "Mutual coupling reduction of a closely spaced four-element MIMO antenna system using discrete mushrooms," *IEEE Trans. Antennas Propag.*, vol. 64, no. 10, pp. 3060–3067, Oct. 2016.

[30] C. Y. Chiu, C. Cheng, R. D. Murch, and C. R. Rowell, "Reduction of mutual coupling between closely-packed antenna elements," *IEEE Trans. Antennas Propag.*, vol. 55, no. 6, pp. 1732–1738, Jun. 2007.

[31] D. Guha, M. Biswas, and Y. M. M. Antar, "Microstrip patch antenna with defected ground structure for cross polarization suppression," *IEEE Antennas Wireless Propag. Lett.*, vol. 4, pp. 455–458, 2005.

[32] C. Kumar and D. Guha, "Nature of cross-polarized radiations from probe-fed circular microstrip antennas and their suppression using different geometries of defected ground structure (DGS)," *IEEE Trans. Antennas Propag.*, vol. 60, no. 1, pp. 92–101, Jan. 2012.

[33] ——, "Asymmetric geometry of defected ground structure for rectangular microstrip: A new approach to reduce its cross-polarized fields," *IEEE Trans. Antennas Propag.*, vol. 64, no. 6, pp. 2503–2506, Jun. 2016.

[34] P. Sharma and K. Gupta, "Analysis and optimized design of single feed circularly polarized microstrip antennas," *IEEE Trans. Antennas Propag.*, vol. 31, no. 6, pp. 949–955, Nov. 1983.

[35] K. Tong and T. Wong, "Circularly polarized U-slot antenna," *IEEE Trans. Antennas Propag.*, vol. 55, no. 8, pp. 2382–2385, Aug. 2007.

[36] H. Zhang, Y. Li, X. Chen, Y. Fu, and N. Yuan, "Design of circular/dual-frequency linear polarization antennas based on the anisotropic complementary split ring resonator," *IEEE Trans. Antennas Propag.*, vol. 57, no. 10, pp. 3352–3355, Oct. 2009.

[37] Nasimuddin, X. Qing, and Z. N. Chen, "Compact asymmetric-slit microstrip antennas for circular polarization," *IEEE Trans. Antennas Propag.*, vol. 59, no. 1, pp. 285–288, Jan. 2011.

[38] Y. Li, Z. N. Chen, X. Qing, Z. Zhang, J. Xu, and Z. Feng, "Axial ratio bandwidth enhancement of 60-GHz substrate integrated waveguide-fed circularly polarized LTCC antenna array," *IEEE Trans. Antennas Propag.*, vol. 60, no. 10, pp. 4619–4626, Oct. 2012.

[39] C. Deng, Y. Li, Z. Zhang, G. Pan, and Z. Feng, "Dual-band circularly polarized rotated patch antenna with a parasitic circular patch loading," *IEEE Antennas Wireless Propag. Lett.*, vol. 12, pp. 492–495, 2013.

[40] X. L. Bao and M. J. Ammann, "Dual-frequency circularly-polarized patch antenna with compact size and small frequency ratio," *IEEE Trans. Antennas Propag.*, vol. 55, no. 7, pp. 2104–2107, Jul. 2007.

[41] J. S. Row, "Design of aperture-coupled annular-ring microstrip antennas for circular polarization," *IEEE Trans. Antennas Propag.*, vol. 53, no. 5, pp. 1779–1784, May 2005.

[42] W. Yoon, J. Baik, H. Lee, S. Pyo, S. Han, and Y. Kim, "A reconfigurable circularly polarized microstrip antenna with a slotted ground plane," *IEEE Antennas Propag. Mag.*, vol. 9, pp. 1161–1164, 2010.

[43] X. Yang, B. Shao, F. Yang, A. Z. Elsherbeni, and B. Gong, "A polarization reconfigurable patch antenna with loop slots on the ground plane," *IEEE Antennas Propag. Mag.*, vol. 11, pp. 69–72, 2012.

[44] P. Lotfi, S. Soltani, and R. D. Murch, "Printed endfire beam-steerable pixel antenna," *IEEE Trans. Antennas Propag.*, vol. 65, no. 8, pp. 3913–3923, Aug. 2017.

[45] C. A. Balanis, *Antenna theory: analysis and design*. John wiley & sons, 2016.

[46] *CST Microwave Studio CST, Version 2019*.

[47] M. Yousefbeiki and J. Perruisseau-Carrier, "A practical technique for accurately modeling reconfigurable lumped components in commercial full-wave solvers [euraap corner]," *IEEE Antennas Propag. Mag.*, vol. 54, no. 5, pp. 298–303, Oct. 2012.

[48] S. Farsi, H. Aliakbarian, D. Schreurs, B. Nauwelaers, and G. A. E. Vandenbosch, "Mutual coupling reduction between planar antennas by using a simple microstrip U-section," *IEEE Antennas Wireless Propag. Lett.*, vol. 11, pp. 1501–1503, 2012.

[49] A. Habashi, J. Nourinia, and C. Ghobadi, "Mutual coupling reduction between very closely spaced patch antennas using low-profile folded split-ring resonators (FSRRs)," *IEEE Antennas Wireless Propag. Lett.*, vol. 10, pp. 862–865, 2011.

[50] T. Huynh and K. F. Lee, "Cross polarization characteristics of rectangular patch antennas," in *Proc. IEEE Int. Symp. Antennas Propag.*, Jun. 1988, pp. 708–711 vol.2.

[51] K. Lee, K. Luk, and P. Tam, "Crosspolarisation characteristics of circular patch antennas," *Electron. Lett.*, vol. 28, no. 6, pp. 587–589, Mar. 1992.

[52] A. Petosa, A. Ittipiboon, and N. Gagnon, "Suppression of unwanted probe radiation in wideband probe-fed microstrip patches," *Electron. Lett.*, vol. 35, no. 5, pp. 355–357, Mar. 1999.

[53] A. Ghosh, D. Ghosh, S. Chattopadhyay, and L. L. K. Singh, "Rectangular microstrip antenna on slot-type defected ground for reduced cross-polarized radiation," *IEEE Antennas Wireless Propag. Lett.*, vol. 14, pp. 321–324, 2015.

[54] C. Kumar and D. Guha, "Defected ground structure (DGS)-integrated rectangular microstrip patch for improved polarisation purity with wide impedance bandwidth," *IET Microw. Antennas Propag.*, vol. 8, no. 8, pp. 589–596, Jun. 2014.